MECHANISMS AND MODELLING OF FLOW-LIKE LANDSLIDES IMPACTING AGAINST PROTECTION STRUCTURES

Angela Di Perna, Sabatino Cuomo
University of Salerno, Italy
adiperna@unisa.it, scuomo@unisa.it

Mario Martinelli
Deltares, Delft, The Netherlands
Mario.Martinelli@deltares.nl

Abstract

Fully coupled hydro-mechanical large deformation models may greatly help in properly simulating the complex interaction between flow-like landslides and protection structures during the dynamic impact process. Many researchers have employed so far either experiments or numerical methods, but the evaluation of the impact forces on the mitigation structures remains difficult especially if the solid-fluid interaction within the flow is considered. While the impacting flowing mass exhibits large deformation during both the propagation and the impact stages, with relevant interaction between its solid skeleton and interstitial water, the impacted body may evolve from small to large deformations during the impact. A suitable approach can be based on a Conceptual Model (CM) and use of Material Point Method (MPM), with the variety of possible interaction mechanisms also considered. In this work, the key features of the impacting mass are taken into account, namely the velocity, impact height, non-zero pore water pressures and frictional behavior of the flow. For the barrier, the geometric and mechanical characteristics are assessed in relation to the materials typically used for such constructions. The numerical results allow estimating the kinematics of the involved masses during the impact, providing also new general insights on Landslide-Structure-Interaction (LSI) mechanisms, as well as specific results for the temporal trend of liquid pressure inside the flow, barrier displacements, overtopping volumes in several design scenarios.

1. Introduction

Understanding the impact mechanisms of flow-like landslides against artificial barriers is still an open issue in the scientific literature. Massive protection structures, such as reinforced embankments, have been used for rockfalls aimed to reduce the kinetic energy of boulders. However, they could be also a reasonable solution for stopping or deviating the propagation of flow-like landslides. In this regard, the assessment of hydromechanical interaction of the landslide body, which is a mixture of solid skeleton saturated with water, still poses scientific issues (Cuomo et al., 2021a). Thus, a proper conceptual model for the Landslide-Structure-Interaction (*LSI*) mechanisms must be fed with a multiphase approach and a large deformation formulation to properly simulate the kinematics of the problem (Cuomo et al., 2021b). A contribution is here provided proposing first a Conceptual Model (*CM*) and then using an innovative numerical approach, named Material Point Method (MPM), for landslides of flow-type impacting different types of protection structures, shaped as artificial embankments, made of coarse-grained soil layers wrapped by high tenacity polyester (*PET*) geogrids (Cuomo et al.,2019). It will be shown that the soil-fluid interaction influences the impact mechanism, the kinematics of the flow, and the spatio-temporal evolution of the impact pressure against the structure.

2. Conceptual Model (CM) for Landslide-Structure-Interaction (LSI)

The impact mechanism of a flow against an obstacle has been investigated by different approaches, mostly experimental and numerical. In the relatively simple case of a flow impacting a vertical barrier,

a wide set of laboratory experiments on dry granular flows allowed Faug (2015) to propose the so-called phase-diagram based on: (i) Froude number ($Fr = v/\sqrt{gh}$) and (ii) obstacle height relative to the flow depth (H/h). The diagram comprises four mechanisms: a) Dead zone (i.e. gradual accumulation of material behind the obstacle): this is the case of relatively slow flows ($Fr \approx 1$) impacting relatively small obstacles ($H/h \approx 1$); b) Airborne jet (forming downstream of the obstacle): this stands for rapid flow ($Fr \gg 1$) and obstacle height low ($H/h \ll 1$); c) Standing jumps (propagating downstream of the obstacle with steady-state conditions): for rapid flow ($Fr \gg 1$); d) Bores (a granular jump hits the obstacle and propagates upstream of it): in the case of a rapid flow ($Fr \gg 1$) hitting a wall spanning the entire width of the flow ($H/h \gg 1$) with unsteady conditions.

The Conceptual model (CM) here proposed for the landslide-structure interaction (*LSI*) considers an unfixed artificial barrier hit by a flow-like landslide mass (Fig. 1). The latter is assumed with the following features: initial velocity $v_{1,0}$, density ρ_m, length L_1, depth h, unitary width, non-zero pore-water pressure p_L and frictional behaviour along the base ground equal to $\tan\varphi_b$. The geometric characteristics of the barrier (i.e, greater base B, smaller base b, height H, inclination of the impacted side β) are considered in relation to the materials typically used for such constructions. Before the landslide reaches the barrier, i.e. during the propagation stage, the *LSI* problem is governed by the basal frictional force F_1 (Eq. 1), since this force controls the amount of entrainment and velocity reduction of flow, resulting in a increase/decrease of the impact forces. Once the flow hits against the barrier, additional stress (mostly horizontally oriented) are produced at the impacted side of the barrier. For the action-reaction principle, the mutual impact forces F_2 between the landslide and the barrier are equal and opposite. Such mutual stress makes: (i) the flow to decelerate and (ii) the barrier to slip along the base and to deform itself, as shown in Fig. 1. The evaluation of the impact forces (Eq. 2) is fundamental to assess the structural characteristics needed for the correct design of the barrier.

It is worth noting that the flow can go beyond the barrier during the impact, generating an additional force F_3 on the structure (Eq. 3), mainly dependent on the flow-barrier frictional contact ($\tan\delta$).

After this impulsive stage of the *LSI*, then problem is mostly governed by inertial force F_4 (Eq. 4), which depends on the amount of friction mobilized at the base of the barrier ($\tan\delta_b$). The final displacement $\varDelta x$ of the barrier is obtained from the equality between the amount of energy that has been transferred to the barrier by the flow and the amount of energy dissipated by friction.
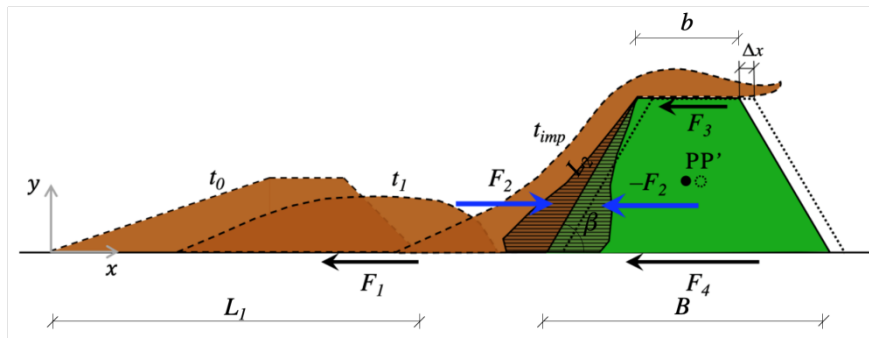

Fig. 1. Schematic for the Landslide-Structure-Interaction (LSI)

$$F_1(t) = \int_0^{L_1(t)} \rho_m g h(x,t) \tan\varphi_b \, dx \tag{1}$$

$$F_2(t) = \int_0^{L_2} \rho_m a(t) h(x,t) sen\beta dx \tag{2}$$

$$F_3(t) = \int_0^{b} \rho_m g h(x,t) \tan\delta \, dx \tag{3}$$

$$F_4(t) = \frac{1}{2}\rho_b g H(b+B)\tan\delta_b + \int_0^{L_2} \rho_m a(t) h(x,t) cos\beta \tan\delta_b \, dx + \int_0^{b} \rho_m g h(x,t) \tan\delta_b \, dx \tag{4}$$

3. Modelling

3.1 Two-phase single-point MPM formulation

The hydromechanical coupling, namely the interaction between solid and liquid in a saturated soil, is here tackled through the *two-phase single-point* formulation (Jassim et al. 2013; Ceccato et al., 2018; Fern et al., 2019). It means that only one set of computational material points is used, which store the information about both the solid and liquid phases. The velocity field of solid $\mathbf{v}_S$ and liquid $\mathbf{v}_L$ phases are both used, but the material points move throughout the mesh with the kinematics of the solid skeleton.

The accelerations of the two phases are the primary unknowns: the solid acceleration $\mathbf{a}_S$, which is calculated from the dynamic momentum balance of the solid phase (Eq. 5), and the liquid acceleration $\mathbf{a}_L$, which is obtained by solving the dynamic momentum balance of the liquid phase (Eq. 6). The interaction force between solid and liquid phases is governed by Darcy's law (Eq. 7). These equations are solved numerically at the grid nodes considering the Galerkin method (Luo et al., 2008) with standard nodal shape functions and their solutions are used to update the MPs velocities and momentum of each phase. The strain rate $\dot{\boldsymbol{\varepsilon}}$ of MPs is computed from the nodal velocities obtained from the nodal momentum.

$$n_S \rho_S \mathbf{a}_S = \nabla \cdot (\sigma - n p_L \mathbf{I}) + (\rho_m - n \rho_L) \mathbf{b} + \mathbf{f}_d \tag{5}$$

$$\rho_L \mathbf{a}_L = \nabla p_L - \mathbf{f}_d \tag{6}$$

$$\mathbf{f}_d = n \mu_L / k \cdot (\mathbf{v}_L - \mathbf{v}_S) \tag{7}$$

The resolution of solid and liquid constitutive laws (Eqs. 8-9) allows calculating the increment of effective stress $d\sigma'$ and excess pore pressure dp_L, respectively. The mass balance equation of the solid skeleton is then used to update the porosity of each MP (Eq. 10), while the total mass balance serves to compute the volumetric strain rate of the liquid phase (Eq. 11) since fluxes due to spatial variations of liquid mass are neglected ($\nabla n \rho_L = 0$).

$$d\boldsymbol{\sigma}' = \mathbf{D} \cdot d\boldsymbol{\varepsilon} \tag{8}$$

$$dp_L = \mathbf{K}_L \cdot d\varepsilon_{vol} \tag{9}$$

$$Dn/Dt = n_S \nabla \cdot \mathbf{v}_S = \mathbf{0} \tag{10}$$

$$D\varepsilon_{vol}/Dt = n_S/n \, \nabla \cdot \mathbf{v}_S + \nabla \cdot \mathbf{v}_L \tag{11}$$

In the two-phase single-point formulation the liquid mass, and consequently the mass of the mixture, is not constant in each material point but can vary depending on porosity changes. Fluxes due to spatial variations of liquid mass are here neglected and Darcy's law is used to model solid-liquid interaction forces. The water is assumed linearly compressible via the bulk modulus of the fluid $\mathbf{K}_L$ and shear stresses in the liquid phase are neglected. However, this formulation proves to be suitable for studying flow-structure-interaction (Cuomo et al., 2021).

The sliding of the flowing mass on the rigid material (i.e. the barrier) is handled by a frictional Mohr-Coulomb strength criterion. The contact formulation was used to ensure that no interpenetration occurs, and the tangential forces are compatible with the shear strength along the contact. The reaction force acting on the structure at node *j* was calculated as in Eq. 12.

$$F_j(t) = m_{j,S} \Delta a_{S,contact} + m_{j,L} \Delta a_{L,contact} \tag{12}$$

The terms $\Delta a_{S,contact}$ and $\Delta a_{L,contact}$ are the change in acceleration induced by the contact formulation, for both solid and liquid phase, and $m_{i,S}$ and $m_{i,L}$ are the corresponding nodal masses. The total reaction force is the integral of the nodal reaction forces along the barrier.

3.2 Examples

Trying to schematize the problem in a simple but realistic way, multiple materials should be considered such as: the flow-like landslide, the protection barrier, and the base soil. The latter is necessary to ensure the frictional contact at the base of the moving barrier (Fig. 2). It is quite difficult to propose a standard landslide configuration as initial condition since it must represent the shape of the flow at a certain time of its propagation stage. As known, this configuration strongly depends on the flow path topography and on the geomorphological conditions that can vary from site to site. However, many studies have demonstrated that the front is often higher than the rear portion due to friction with the ground topography (Thouret et al., 2020, among others). For this reason, the chosen initial configuration of the landslide is characterized by a 45°-inclined front and a tail of length equal to three times the flow height, with a number (i) of squares placed between the head and tail portions.

For the barrier it is assumed: dry material, frictional contact at base and rigid behavior. This last hypothesis relates to the construction mode typically used for such kind of barrier, which involve the use of 0.6–0.7 m thick layers of coarse materials reinforced through geosynthetics (usually geogrids) with high tensile strength and wrapped around the facing of the barrier. In fact, recent studies have outlined that local deformation of the barrier or relative horizontal shifting of the layers may occur under the impact of flows (Cuomo et al., 2019), although the horizontal displacement along the base is the prevailing limit state of the barrier. This finding combined to the fact that both the core soil and the geogrids are very resistant materials makes the structure experiencing stress levels much lower than the ultimate values in most parts of the structure. Moreover, the frictional resistance along the base is set as the 80% of the strength properties of the subsoil base material (Cuomo et al., 2019).

Examples are here presented to discuss the influence of the ratio H/h and the slope β of the impacted side of the barrier on LSI mechanisms and spatio-temporal evolution of pore water pressure.

The mass of the barrier is kept constant, as well as other some other features (Fig. 2): $L_1=21$ m; $i=3$; $h=3$ m; V_1 (flow volume) $=45$ m³/m; $v_{0,1}= 10$ m/s; $d=3$ m. Other geometric features of both the landslide and the barrier have been changed in three different impact scenarios (a-b-c): $\beta=60°$(a)-72°(b)-80°(c); $L_2=6.95$(a)-7.87 (b)-6.08(c) m; $B=11$(a)-8.38(b)-8.50 (c) m; $b=4$(a)-3.63(b)-6.50(c) m; $H=6$(a-c)-7.50(b) m.
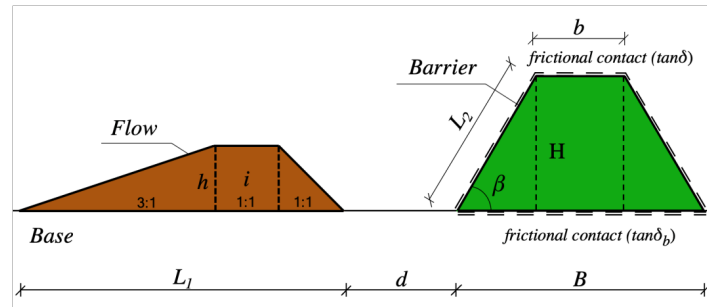

Fig. 2. Geometric schematization of the problem

Based on the Conceptual Model here proposed, the diagram of Faug (2015) is used to predict the type of impact mechanism for each scenario (Table 1), and to preliminarily assess the efficiency of the barrier in intercepting the propagation of the flow under different impact conditions.

Table 1. Expected impact mechanism.

ID	Fr $(-)$	H/h $(-)$	Impact mechanism
a-c	1.84	2.0	Standing jump
b	1.84	2.5	Standing jump

Numerical modeling is used to validate such assessment, to provide insights in the mechanics of LSI, and to evaluate the behaviour of both the flow and the barrier. MPM has been used. The mechanical properties of the saturated flow mass and the friction angle at the contact with the barrier are: $\rho_m=1800$ kg/m^3; n (porosity)$=0.4$; K_0 (earth's pressure coefficient)$=0.66$; φ' (effective friction angle)$=20°$; c' (effective cohesion)$=0$; E' (Young modulus)$=2$ MPa; v (Poisson's ratio)$=0.25$; k (hydraulic conductivity)$=10^{-4}$ m/s; μ_L (liquid viscosity)$=10^{-3}$ Pas; K_L (liquid bulk modulus)$=30$ MPa; ρ_b (barrier density)$=2000$ kg/m^3; $tan(\delta)=0.29$; $tan(\delta_b)=0.29$. The flow mass is a saturated mixture with a linear vertical distribution of the initial pore-water pressure. The computational unstructured mesh is made of 20515 triangular 3-noded elements with dimensions ranging from 0.20 to 1.00 m.

Selected results are here shown for the spatial distribution of pore-water pressure at different time lapses (Fig. 3) for the different cases (a-b-c).

During the early stage of the impact, the initial pore-water pressure (< 30 kPa) changes over time, with the maximum value in the first instants of the impact process ($t = 1$ s) and then diminishing with time down to nil in some cases. However, the maximum of pore-water pressure ($p_{L,max}$) reaches different values depending on the type of barrier. At $t = 2$ s, the flow goes beyond the barrier forming a prolonged jet. Liquid pressure is decreasing, indicating that we are in the decay zone of the impact force diagram. Subsequently ($4 s < t < 6 s$), the flow loses more and more energy and falls downwards in a similar way in all the cases. The numerical results validate that the expected impact mechanism, i.e. "*standing jump*" (Table 1), actually occur in all the three cases (where the barrier has the same volume but different aspect ratio).

However, even if the impact mechanism is practically the same, the amount of flow that propagates beyond the barrier depends on the type of barrier. This is related to the different of pore water pressure generated inside the flow at the impact.
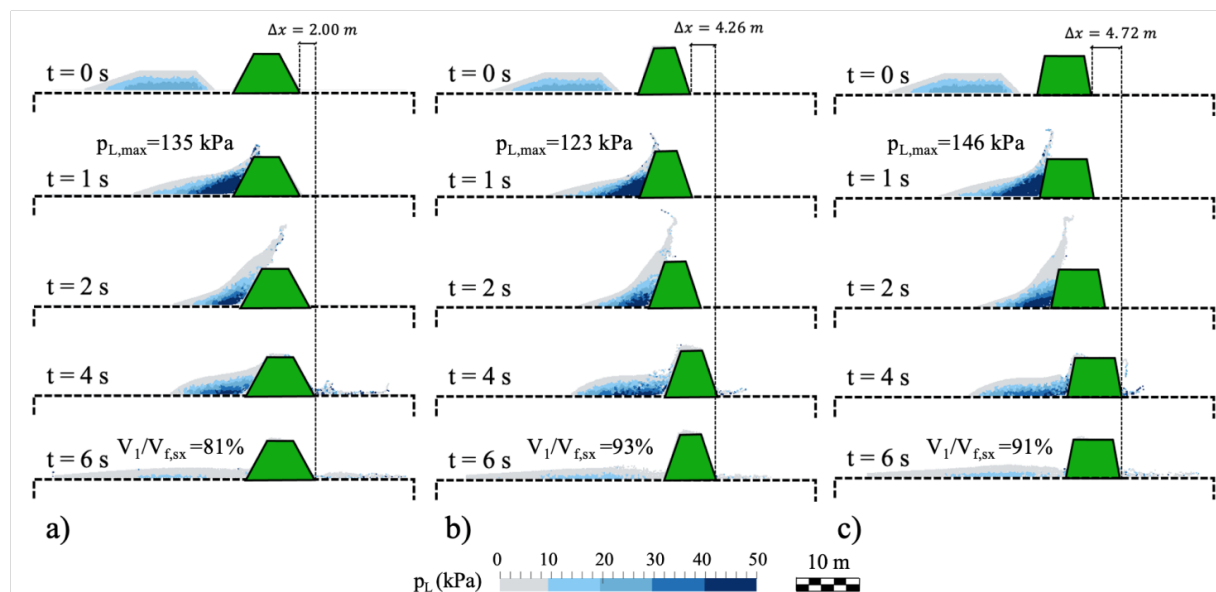

Fig. 3 Pore-water pressure distribution for unfixed artificial barriers:
(a) H/h=2; β=60°; (b) H/h=2.5; β=72°; (c) H/h=2; β=80°.

This outcome confirms previous research showing that an increase in pore-water pressure favors the overtopping of a barrier (Song et al., 2017; Zhou et al., 2018). In fact, the results also show that the inclination β and the barrier height relative to the flow depth (H/h) play a significant role in the generation of excess pore-water pressure. Other insights relate to Fig. 3a: a higher barrier (fig. 3b) makes a reduction of $p_{L,max}$ from 135 kPa to 123 kPa; while a more inclined impact side (Fig. 3c) gives a higher value equal to 146 kPa. The amount of material that is retained by the barrier ($V_{f,sx}$) increases with the inclination β and height H of the barrier. The final displacement exhibited by the barrier is longer when the inclination β increases and for shorter base of the barrier.

4. Conclusions

A Conceptual Model (CM) has been here proposed for the analysis of Landslide-Structure-Interaction (LSI) mechanisms of a flow-like landslide impacting a deformable movable barrier. First, the problem has been schematized and the potential flow-obstacle interaction mechanism assessed based on the combination of the flow-obstacle geometry and the kinematic features of the flow. Then, a multiphase approach and a large deformation formulation based on Material Point Method (MPM) numerical technique has been used to properly simulate the complex hydro-mechanical interaction of the flow against the barrier, thus allowing a better understanding of the impact mechanisms. It has been also noted that some geometric features (such as the ratio H/h and the inclination β) contribute to reduce the build-up in pore water pressures inside the landslide mass, thus preventing the overtopping of the barrier. Future studies will allow to fully investigate the feasibility of such protection structures.

5. Acknowledgments

References

Ceccato, F., Yerro A., and Martinelli M. (2018). Modelling soil-water interaction with the Material Point Method. Evaluation of single-point and double-point formulations. NUMGE, 25-29 June. Porto, Portugal

Cuomo, S., Moretti, S., Frigo, L., Aversa, S. (2019). Deformation mechanisms of deformable geosynthetics-reinforced barriers (DGRB) impacted by debris avalanches. Bulletin of Engineering Geology and the Environment, 1-14. https://doi.org/10.1007/s10064-019-01589-w

Cuomo, S., Di Perna, A., Martinelli, M. (2021a). MPM hydro-mechanical modelling of flows impacting rigid walls. Canadian Geotechnical Journal, https://doi.org/10.1139/cgj-2020-0344

Cuomo, S., Di Perna, A., & Martinelli, M. (2021b). Modelling the spatio-temporal evolution of a rainfall-induced retrogressive landslide in an unsaturated slope. Engineering Geology, 106371.

Fern, J., Rohe, A., Soga, K., & Alonso, E. (Eds.). (2019). The material point method for geotechnical engineering: a practical guide. CRC Press.

Jassim, I., Stolle, D., and Vermeer, P. (2013). Two-phase dynamic analysis by material point method. International journal for numerical and analytical methods in geomechanics, 37(15), 2502-2522.

Luo, H., Baum, J. D., and Löhner, R. 2008. A discontinuous Galerkin method based on a Taylor basis for the compressible flows on arbitrary grids. Journal of Computational Physics, 227(20), 8875-8893.

Thouret, J. C., Antoine, S., Magill, C., and Ollier, C. (2020). Lahars and debris flows: Characteristics and impacts. Earth-Science Reviews, 201, 103003.

Song, D., Ng, C. W. W., Choi, C. E., Zhou, G. G., Kwan, J. S., and Koo, R. C. H. 2017. Influence of debris flow solid fraction on rigid barrier impact. Canadian geotechnical journal, 54(10), 1421-1434.

Zhou, G. G. D., Song, D., Choi, C. E., Pasuto, A., Sun, Q. C., and Dai, D. F. (2018). Surge impact behavior of granular flows: effects of water content. Landslides, 15(4), 695-709.